

Two-photon Imaging of Glutathione Levels in Intact Brain Indicates Enhanced Redox Buffering in Developing Neurons and Cells at the Cerebrospinal Fluid and Blood-Brain Interface*

Received for publication, February 17, 2006, and in revised form, April 17, 2006 Published, JBC Papers in Press, April 19, 2006, DOI 10.1074/jbc.M601567200

Xiaojian Sun[‡], Andy Y. Shih^{‡1}, Helge C. Johannssen^{‡2}, Heidi Erb[‡], Ping Li[‡], and Timothy H. Murphy^{‡53}

From the Departments of [‡]Psychiatry and [§]Physiology, Kinsmen Laboratory of Neurological Research and Brain Research Centre, University of British Columbia, Vancouver V6T 1Z3, British Columbia, Canada

Glutathione is the major cellular thiol present in mammalian cells and is critical for maintenance of redox homeostasis. However, current assay systems for glutathione lack application to intact animal tissues. To map the levels of glutathione in intact brain with cellular resolution (acute tissue slices and live animals), we have used two-photon imaging of monochlorobimane fluorescence, a selective enzyme-mediated marker for reduced glutathione. Previously, *in vitro* experiments using purified components and cultured glial cells attributed cellular monochlorobimane fluorescence to a glutathione *S*-transferase-dependent reaction with GSH. Our results indicate that cells at the cerebrospinal fluid or blood-brain interface, such as lateral ventricle ependymal cells (2.73 ± 0.56 mM; glutathione), meningeal cells (1.45 ± 0.09 mM), and astroglia (0.91 ± 0.08 mM), contain high levels of glutathione. In comparison, layer II cortical neurons contained 20% (0.21 ± 0.02 mM) the glutathione content of nearby astrocytes. Neuronal glutathione labeling increased 250% by the addition of the cell-permeable glutathione precursor *N*-acetylcysteine indicating that the monochlorobimane level or glutathione *S*-transferase activity within neurons was not limiting. Regional mapping showed that glutathione was highest in cells lining the lateral ventricles, specifically ependymal cells and the subventricular zone, suggesting a possible function for glutathione in oxidant homeostasis of developing neuronal progenitors. Consistently, developing neurons in the subgranular zone of dentate gyrus contained 3-fold more glutathione than older neurons found in the neighboring granular layer. In conclusion, mapping of glutathione levels in intact brain demonstrates a unique role for enhanced redox potential in developing neurons and cells at the cerebrospinal fluid and blood-brain interface.

The tripeptide glutathione (GSH; γ -L-glutamyl-L-cysteinylglycine) is the most abundant low molecular weight thiol in mammalian cells and constitutes a major cellular defense against reactive oxygen species. Deficiency in the GSH system has been linked to neuronal loss dur-

ing progression of neurodegenerative diseases, such as Parkinson, Alzheimer, Huntington, and amyotrophic lateral sclerosis (1–3), as well as acute conditions such as spinal cord injury (4) and stroke (5–7). Although reactive oxygen species accumulation has been implicated in these disorders, examination of GSH levels in previous studies has largely been restricted to enzymatic assays and fluorescent probes that are only applicable in neuronal and glial cell cultures or brain homogenates. A widely used method for measuring GSH in cultured cells and tissue homogenates employs monochlorobimane (MCB)⁴ (8), a normally nonfluorescent dye that when conjugated to reduced GSH by intracellular glutathione *S*-transferases (GSTs) forms adducts that can be measured fluorometrically. Recently, investigators have established that GSH in epidermal cells of intact *Arabidopsis* roots can be elegantly and quantitatively measured by two-photon laser scanning microscopy (TPLSM) with MCB (9). Accordingly, we now use a similar approach in intact mammalian brain to directly monitor GSH levels in different tissues.

Data on GSH concentrations in different brain areas of various species obtained using chemical techniques have been summarized (10). However, because these results were derived from tissue homogenates, they only provide information on the average GSH content. It is also conceivable that other techniques such as thiol-reactive probes (11) may lack specificity for GSH or suffer from the disposition of thiols/GSH changing in response to animal sacrifice and/or fixation. Furthermore, studies from cultured brain cells are potentially affected by media constituents that contain high levels of GSH precursors such as cystine, present at 100 μ M in minimal essential media but less than 1 mM in cerebrospinal fluid *in vivo* (12). Here we show that MCB is a specific probe for GSH labeling in brain tissues, and TPLSM can be used to image GSH content in various brain regions at the cellular level. In our assay, the extracellular environment contains a large reservoir of MCB (compared with intracellular GSH), and therefore the reaction between MCB and GSH is first order and can be described by a single exponential function. As we have shown for cell cultures using plate reader assays (13), we can now use TPLSM imaging *in situ* to measure several kinetic parameters of GSH metabolism such as its conjugation rate by GST and total GSH-MCB content. By applying TPLSM to rat brain slices and neocortex of live anesthetized mice, we have found that GSH is enriched in meninges, lateral ependymal cells, astrocytes, and immature neurons in dentate gyrus. Neocortical neurons in slices from mature animals can

* This work was supported in part by a Canadian Institutes of Health Research training grant (to X. S.), a Canadian Institutes of Health Research Canadian Graduate Scholarship (to A. Y. S.), and an operating grant from the Heart and Stroke Foundation of British Columbia and Yukon (to T. H. M.). The costs of publication of this article were defrayed in part by the payment of page charges. This article must therefore be hereby marked "advertisement" in accordance with 18 U.S.C. Section 1734 solely to indicate this fact.

¹ Recipient of a Michael Smith Foundation for Health Research (MSFHR) studentship.

² Present address: Dept. of Neurophysiology, Brain Research Institute, University of Zurich, Zurich, Switzerland.

³ Supported by the Canadian Stroke Network and is an MSFHR Senior Scholar. To whom correspondence should be addressed: 4N1-2255 Wesbrook Mall, University of British Columbia, Vancouver, British Columbia V6T 1Z3, Canada. Tel.: 604-822-0705; Fax: 604-822-7981; E-mail: thmurphy@interchange.ubc.ca.

⁴ The abbreviations used are: MCB, monochlorobimane; GST, glutathione *S*-transferase; TPLSM, two-photon laser scanning microscopy; PBS, phosphate-buffered saline; ACSF, artificial cerebral spinal fluid; FITC, fluorescein isothiocyanate; BSO, L-buthionine sulfoximine; DCX, double cortin; PI, propidium iodide; Mrp, multidrug resistance protein; CSF, cerebrospinal fluid; SR 101, sulforhodamine 101; PMT, photo-multiplier tube.

be labeled by MCB but at a much lower level of fluorescence, suggesting that glial, meningeal, and ependymal cell sources may play a dominant role in buffering brain oxidative stress.

MATERIALS AND METHODS

Chemicals—All reagents were purchased from Sigma unless mentioned otherwise. Monochlorobimane was purchased from either Fluka or Molecular Probes and made as a 100 mM stock solution in Me₂SO and stored at -20°C . Sulforhodamine 101 (SR 101) was prepared as a 10 mM stock solution in Me₂SO and also stored at -20°C . Propidium iodide was purchased from Molecular Probes and made as a 10 mM solution in PBS and stored at 4°C . Primary antibodies used in this study included anti-laminin (rabbit), anti-S-100 β (mouse), and anti-NeuN (mouse, Chemicon). Secondary antibodies included FITC anti-rabbit, FITC anti-mouse, and Alexa 594 anti-mouse (Molecular Probes).

Plate Reader GSH Assay—Fluorometric assays were performed using a plate reader (Fluoroskan; Ascent, FL), $\lambda_{\text{ex}} = 355 \pm 19$ nm and $\lambda_{\text{em}} = 527 \pm 5$ nm. Although these excitation/emission filters are suboptimal for MCB detection, they prevented saturation of the detector within the plate reader permitting linearity between the concentration of MCB-GSH and detected fluorescence over the range associated with the fluorescence values in our measurements. Purified 200 μM GSH and 10 μM MCB were added together, with varying concentrations of purified GST enzyme (0, 0.01, 0.02, and 0.04 units (equine); Sigma). Fluorescence was measured using a plate reader over a 4-h reaction period.

Calibration of the GSH-MCB Fluorescence—A 5 mM stock solution of GSH-MCB was made from 20 mM GSH and 3 mM MCB in the presence of a GST. Excess GSH and GST were used to ensure that all MCB was conjugated. A dilution series of 5, 1.5, 0.5, and 0.15 mM was made from this stock. The standard solutions were contained within *in vitro* cells (glass microcuvettes, inner diameter = 50 μm ; VitroCom) and imaged with two-photon microscopy using identical power settings to those used on brain tissues. This method of GSH-MCB calibration was routinely used in our studies in brain slices.

Rat Brain Slice Preparation—Coronal brain slices were prepared from P15-21 or P1-2 Wistar rats (Charles River Breeding Laboratories, Canada). Under halothane anesthesia, animals were killed, and the brain was quickly removed from the skull and placed in ice-cold cutting solution containing (in mM) 200 sucrose, 2.5 KCl, 0.5 CaCl₂, 26.2 NaHCO₃, 10 MgSO₄·7H₂O, 1 NaH₂PO₄, 11 glucose (pH was maintained at 7.4 by saturation with 95% O₂ and 5% CO₂). Slices (300 μm) were obtained with a vibratome (Leica VT 1000 S) and then transferred to a static bath chamber where they were maintained at room temperature for at least 1 h before imaging. The slices were kept in artificial cerebral spinal fluid (ACSF) containing (in mM) 120 NaCl, 26.2 NaHCO₃, 24.2 glucose, 2.5 KCl, 1.25 NaH₂PO₄, 1 MgCl₂·6H₂O, 2 CaCl₂, saturated with 95% O₂ and 5% CO₂. For imaging, individual slices were transferred to a recording chamber and perfused with ACSF saturated with 95% O₂ and 5% CO₂. MCB was added to the perfusion system at a final concentration of 60 μM . To identify dead cells, we added 10 μM propidium iodide together with MCB.

Animal Preparation for *In Vivo* Imaging—All experiments were approved by the University of British Columbia Animal Care Committee and were conducted in strict accordance with guidelines from the Canadian Council on Animal Care. C57Bl/6 mice were purchased from The Jackson Laboratory (Bar Harbor, ME) and bred at the University of British Columbia animal facilities. Cranial windows for *in vivo* imaging were produced as described previously (14). In brief, mice aged 3–5 months were deeply anesthetized with an intraperitoneal injection of urethane (0.12% w/w, supplemented with 0.02% w/w as needed) (15),

and 20 mM glucose in PBS was supplemented to maintain animal hydration (0.2–0.3 ml, intraperitoneal injection, every 1 h). Body temperature was maintained at 37°C using a feedback-regulated heating pad. An air-powered dental drill was used to produce a $2 \times 2\text{-mm}^2$ cranial window over the somatosensory cortex at coordinates of 0.8 mm from bregma and 2.0 mm lateral, leaving the dura intact. A stainless steel chamber that surrounded the craniotomy was glued to the skull with Crazy Glue (Elmer's Products, Columbus, OH). To reduce movement artifacts, the area between the chamber and the skull was filled with dental acrylic (16). The exposed cortical surface and chamber were filled with 2% (w/v) agarose (diluted in PBS or a HEPES-buffered ACSF) and sealed with a cover glass. For *in vivo* labeling, MCB and SR 101 stocks were dissolved in PBS to a final concentration of 100 μM and applied directly to the exposed brain surface.

Two-photon Microscopy—Two-photon excitation of GSH-MCB conjugates was achieved using a Coherent (Santa Clara, CA) Mira 900 Ti:sapphire laser pumped by a 5-watt Verdi laser tuned to 780 nm. Images were acquired using custom software routines (IgorPro; Wavemetrics, Eugene, OR) and by using an Olympus (Tokyo, Japan) IR-LUMPlanFl water-immersion objective (40 \times ; 0.80 numerical aperture). When MCB was used in combination with SR 101, the laser was operated at 800 nm, and fluorescence was collected using photo-multiplier tube 1 (PMT1) for the GSH-MCB signal (512–562 nm), and PMT2 for the SR 101 signal (620–645 nm). For immunostaining, FITC and Alexa 594 were used as secondary antibody fluorophores. Both fluorophores were excited at 800 nm, and the signals were collected on PMT1 and PMT2, respectively. Excitation power was measured at the objective back aperture. For two-photon imaging of various tissues, the following power settings were used: lateral ventricle ~ 20 – 30 milliwatts, ~ 40 – 50 -milliwatt cortical astrocytes, and 80 – 90 milliwatts for neurons. Power through the objective was at least 50% lower than that measured at the back aperture because of back aperture overfilling and absorbance by glass.

Tissue Fixation and Immunostaining—After MCB labeling and two-photon imaging, slices were fixed with 4% paraformaldehyde in 0.1 M phosphate buffer (pH 7.2) for 1 h. Slices were then rinsed twice with PBS and treated with primary antibody against S-100 β (1:1000 in antibody buffer), NeuN (1:100 in antibody buffer), or laminin (1:500 in antibody buffer) for 48 h at 4°C . The antibody buffer contained 0.1% Triton X-100 and 2% goat serum in PBS. After washing twice with PBS, the slices were incubated with secondary antibodies (FITC anti-rabbit, FITC anti-mouse, and Alexa 594 anti-mouse; diluted 1:200 in antibody buffer) for 48 h in dark at 4°C . After secondary antibody labeling, slices were washed twice with PBS and imaged with two-photon microscopy.

Image Analysis—Image analysis was performed using NIH ImageJ software. To reduce photon and PMT noise, a median filter (radius = 1 or 2) was applied. The fluorescence intensity was converted to GSH-MCB concentration according to a standard curve. For statistical analyses, two-tail paired *t* test or repeated measures one-way analysis of variance was used with GraphPad Prism (version 2.01). Data were expressed as mean \pm S.E.

RESULTS

Specificity of Monochlorobimane Labeling—Currently, MCB is the probe of choice for measuring GSH levels in intact cells. MCB is essentially nonfluorescent in the absence of GSH. In a reaction catalyzed by GST, GSH is conjugated to MCB, generating a product with blue-green fluorescence (17, 18). MCB has advantages over other bimane derivative dyes for measuring GSH, such as monobromobimane and monobromotrimethylammoniumbimane, because it shows very low affinity for

Imaging Glutathione in Intact Brain Indicates Redox Buffers

other low molecular weight or protein thiols (*i.e.* cysteine) (19). Using a plate reader assay, we further tested the specificity of MCB for the reduced form of GSH in *in vitro* experiments using purified GST to catalyze the reaction. In the absence of GST, addition of 200 μM GSH to 10 μM MCB resulted in a modest linear increase in fluorescent product over time (Fig. 1A). Addition of purified GST (0.01–0.04 units) resulted in a robust single exponential phase increase in the fluorescence intensity, indicating that this is an enzyme-catalyzed reaction following first-order kinetics (Fig. 1A). The curve can be fitted with Equation 1,

$$F = F_0 + F_{\text{max}}(1 - \exp(-(t - t_0)/\tau)) \quad (\text{Eq. 1})$$

where F is the fluorescence intensity; F_{max} is the maximum fluorescence intensity, and τ is the time constant of the reaction. The plateau level of the *in vitro* reaction (purified components) was related to the amount of GSH and MCB added, but not GST, whereas the initial conjugation rate was proportional to the GST amount. The time constants of the exponential phase were 1437, 691, and 344 s, respectively, for 0.01, 0.02, and 0.04 units of GST. The GST dependence of this reaction confers the specificity of MCB for labeling GSH. When comparing different cell populations in subsequent brain slices and *in vivo* experiments, we recorded time courses to ensure that all reactions proceeded to completion, and thus GST activity was not a limiting factor.

Because MCB is a membrane-permeable dye (8) and GST is widely expressed in brain cells, such as neurons and glial cells (20), a similar labeling effect should be achievable in brain cells, thus allowing the measurement of cellular GSH content by measuring the fluorescence intensity of the accumulated GSH-MCB product. Our previous experiments have confirmed this by showing that MCB labeling of astrocyte cultures, which had been pretreated with the irreversible GSH synthesis inhibitor L-buthionine sulfoximine (BSO), have a significantly reduced MCB fluorescence at the reaction plateau (13). The reduced fluorescence was not because of a direct effect of the BSO itself because addition of exogenous GSH greatly increased GSH-MCB fluorescence within these cells (13). Consistent with the proposal that the initial rate of GSH conjugation with MCB reflects GST activity and not necessarily GSH levels, we observed that treatment of astrocyte cultures with BSO (to lower the available GSH pool) did not affect the initial GSH-MCB conjugation rate (data not shown). Fortuitously, at room temperature, which was used for all brain slice experiments, the efflux of GSH-MCB conjugates was negligible (cellular fluorescence did not decrease after extensively washing MCB from the perfusate; GSH-MCB concentration in neurons changed from 0.143 ± 0.011 to 0.149 ± 0.020 mM with washout, $p > 0.05$; in astrocytes, it changed from 0.726 ± 0.071 to 0.727 ± 0.065 mM, $p > 0.05$), suggesting that the measured GSH content was not underestimated because of MCB-GSH efflux from the cell. In contrast, in astrocyte cell culture at 37 °C the conjugate was largely effluxed from cells. Astrocyte efflux could be inhibited by treatment with MK571, a blocker of multidrug resistance proteins (Mrps) (13, 21, 22). In brain slice experiments at room temperature, we observed no significant effect of MK571 (50 μM) inhibition of Mrps on MCB fluorescence ($p > 0.05$ from five separate slice experiments). Thus our results confirmed that MCB can be used to label intracellular GSH with the plateau level of fluorescence intensity indicating the cellular GSH content, whereas the initial conjugation rate reflected GST activity.

Feasibility of Two-photon Laser Scanning Microscopy for Measurement of Cellular GSH Levels—GSH-MCB conjugate emits significant fluorescence at 450–575 nm when excited by TPLSM at 780 nm (9). The *in vitro* production of GSH-MCB using purified reagents allowed us to produce defined amounts of GSH-MCB to use as standards in TPLSM experiments. The standard curve indicated that TPLSM was a

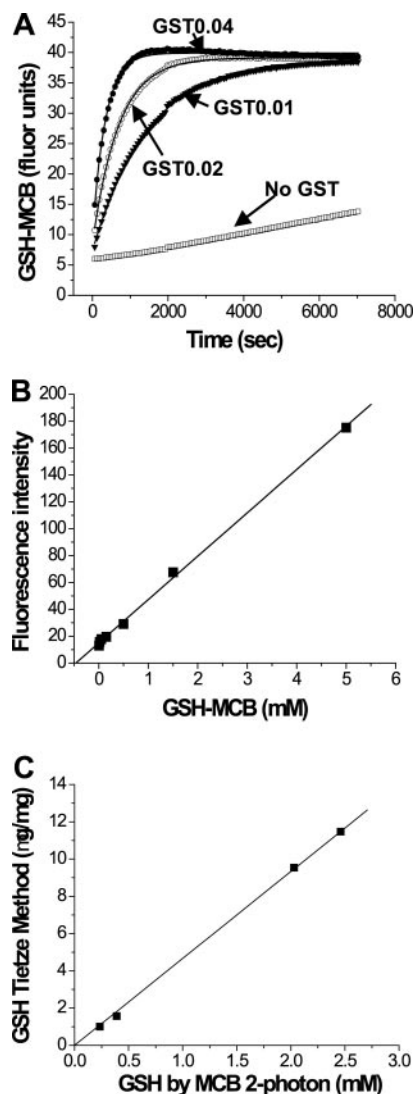


FIGURE 1. MCB labeling of GSH in vitro. A, *in vitro* experiments with the reduced form of GSH (200 μM) and MCB (10 μM) and the indicated amounts of purified GST (0, 0.01, 0.02, and 0.04 units). A low linear increase in MCB fluorescence was observed without GST. Addition of GST led to an exponential phase of MCB-GSH production (fitted with a single exponential curve), in which the reaction time constant was inversely proportional to the units of GST added. The time constants were 1437, 691, and 44 s, respectively, for GST 0.01, 0.02, and 0.04 units. The reaction was carried out at 37 °C. The fluorescence intensity was measured by a plate reader ($\lambda_{\text{ex}} = 355 \pm 38$ nm and $\lambda_{\text{em}} = 527 \pm 5$ nm). B, standard curve for the relationship between fluorescence intensity and GSH-MCB concentration. GSH-MCB solutions of known concentration were made from a GST-catalyzed reaction between the reduced form of GSH and MCB and then filled into Vitrocells (micro-cuvettes) and imaged with two-photon microscopy. Over a range of 0–5 mM, a linear relationship was observed between GSH-MCB concentration and fluorescence ($R^2 = 0.99$). C, a linear relationship ($R^2 = 0.99$) between two-photon imaging of MCB-GSH levels and biochemical assay of total GSH under conditions that suppress or enhance GSH levels. Cultured rat astrocytes were treated with 10 and 3 mM BSO for 16 h to produce the lowest levels of GSH on the graph shown. Higher levels of GSH were observed in untreated cells or cell treated with the cysteine donor *N*-acetylcysteine 1 mM for 90 min, respectively. GSH levels were estimated on sister cultures using either the Tietze biochemical assay (measures total GSH) or the MCB two-photon imaging assay. Standard curves were constructed for both assays, and results were expressed as mg of GSH/mg of protein (Tietze assay) or as a GSH concentration when using the GSH-MCB imaging approach using standards prepared and described in B.

viable technique to measure up to 5 mM concentrations of GSH (Fig. 1B). GSH-MCB standards containing microcuvettes (50 μM path length) were placed on the two-photon microscope and imaged in an identical manner as brain slices. Assuming that the GST-mediated conjugation of GSH with MCB goes to completion, as indicated by our time course analysis, and that little GSH-MCB efflux occurs at room temper-

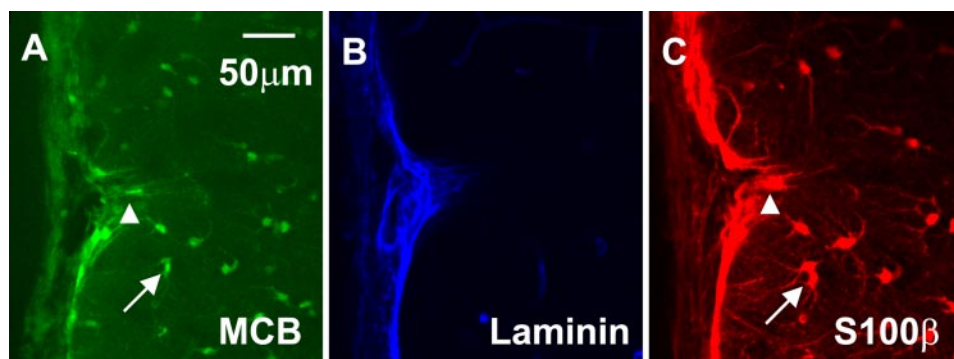


FIGURE 2. **MCB labels the meninges and astrocytes robustly.** *A*, green fluorescence of rat brain slices labeled with MCB. *B*, laminin labeling pattern of the same region, from green detection channel after immunostaining. The MCB signal was completely lost during paraformaldehyde fixation for immunostaining (note very different pattern); therefore, it did not interfere with the secondary antibody (FITC anti-rabbit) signal. For presentation a blue color table was added. *C*, red fluorescence of cells stained with S-100 β as primary antibody and Alexa 594 anti-mouse as secondary antibody. *A* and *C* show that the highly fluorescent MCB-labeled cells are astrocytes. Arrow and arrowhead point to an astrocyte and a perivascular cell labeled by both MCB and S-100 β , respectively. Images were taken using two-photon microscopy of a rat brain slice with a $\times 40$ objective.

ature, we expect the GSH-MCB fluorescence intensity measured by using this method to be proportional to the cellular GSH concentration. To ensure that differences in fluorescence path length do not contribute to the observed differences in GSH levels between cells and tissues, we optically sectioned each cell and made maximal intensity projections over regions of cells that were considerably larger than the axial resolution of the microscope ($< 3 \mu\text{m}$). By choosing these thicker regions of the cell, we assumed that MCB fluorescence intensity is proportional to GSH-MCB concentration and not structure path length or volume (9).

To determine whether two-photon imaging of GSH-MCB fluorescence yields results that are proportional to a classical biochemical assay of total GSH, we compared the GSH level of cultured astrocytes treated with varying concentrations of BSO (0, 3, and 10 μM) or 1 mM *N*-acetylcysteine using either the Tietze method (23) or two-photon imaging (Fig. 1C). As expected, the Tietze method showed that these treatments resulted in cells with graded total GSH content. On parallel cultures treated at room temperature and with MK571 to reduce conjugate efflux, we performed two-photon imaging on the various groups of astrocytes using the same procedures for brain slices. By using standards produced *in vitro*, we converted GSH-MCB fluorescence to an equivalent GSH concentration. Comparison between the various astrocyte treatments indicated remarkable correspondence between the assays ($R^2 = 0.99$) confirming that GSH-MCB fluorescence measured by two-photon imaging is directly proportional to total GSH determined by a classic method of assaying GSH. These results also suggest that the local intracellular environment or organelle sequestration does not have a major effect on the concentration of GSH reported by the two-photon imaging technique.

Meningeal Cells and Astrocytes in Neocortex Are Labeled Intensely by MCB in Rat Brain Slices—After establishing that MCB can be a specific indicator of GSH, we examined the GSH distribution in various brain tissues in acute P15–20 rat slices at room temperature. On the slice surface many unstained cell bodies appeared as black holes and were labeled by the polar membrane-impermeable marker propidium iodide (PI) (24) indicating that they had ruptured membranes (data not shown). As we imaged deeper into slices (over 20–30 μm deep), there was a lower incidence of unstained cell bodies, indicating that cell death at the slice surface was caused by vibratome sectioning (data not shown). Within live brain slices MCB robustly labeled the meninges and a subpopulation of cells in neocortex with astroglial morphology, as well as perivascular cells (Fig. 2A). In order to verify the cell type of these GSH-positive cells, we performed immunostaining with the calcium-binding protein S-100 β , a specific marker of astrocytes in fixed slices (25). Importantly, to reduce the possible changes in GSH distribution

following fixation, we obtained all GSH-MCB localization data from live tissues. To label astrocytes in fixed tissues, we used antibodies to S-100 β because markers such as glial fibrillary acidic protein fail to label all astrocyte cell populations (26). Because MCB tends to leak out of cells in paraformaldehyde-fixed tissue, we also stained the slices with either laminin, which is a major component of basement membranes in blood vessels, or PI as landmarks to locate the same region from which we had imaged GSH-MCB (Fig. 2B). As fixation of slices caused some distortion of cell position, we examined co-localization based on cell morphology and the relative position of cells over a relatively small area. Most of the highly fluorescent MCB-labeled neocortical cells were S-100 β -positive and thus were presumably astrocytes (75% MCB/S-100 β co-staining, $n = 47$, 2 animals with 2 slices each; see Fig. 2C). The perivascular cells were also S-100 β -positive astrocytes with their end feet tightly ensheathing the vessel wall (Fig. 2, A and C, arrowhead). An increased level of GSH in astrocytes is consistent with their crucial role in the antioxidant defense of the brain (10, 27, 28). For example, astrocytes can protect neurons from oxidative stress via GSH-dependent mechanisms and therefore would be expected to require an intracellular reservoir of GSH (29–32).

In addition to astrocytes, we also found that meningeal cells (most likely pial and arachnoid cell layers) were intensely labeled by MCB, indicating a very high GSH level. Meningeal cells have received little attention with respect to neuroprotection except for their role in the regulation of blood flow and the blood-cerebrospinal fluid (CSF) barrier (33, 34). Related structures such as the choroid plexus have been long known to filter and remove exogenous and endogenous toxins from the CSF (35). Recently, Sato *et al.* (36) found that the high affinity cystine-glutamate antiporter system x_c^- (xCT) is expressed at particularly high levels in meninges. In many cell types, the uptake of cystine is the rate-limiting step for GSH synthesis. Meningeal cells may use xCT-dependent cystine uptake as an efficient means to supply cysteine for maintenance of a large GSH pool. This enhanced GSH production by the meninges may play an important role in buffering brain oxidative stress. Consistent with this proposal, we found meningeal cells to be more potent than cortical astrocytes in protecting neurons from an *in vitro* oxidative stress model.⁵

MCB Labeling of Neurons in Slices Is Much Weaker than Labeling of Astrocytes—When imaging deeper layers of the neocortex in P15–20 rat coronal slices, such as layer II and III (Fig. 3A), we identified another group of cells that were MCB-labeled but with lower fluorescence.

⁵ A. Y. Shih, X. Sun, H. Erb, and T. H. Murphy, manuscript in preparation.

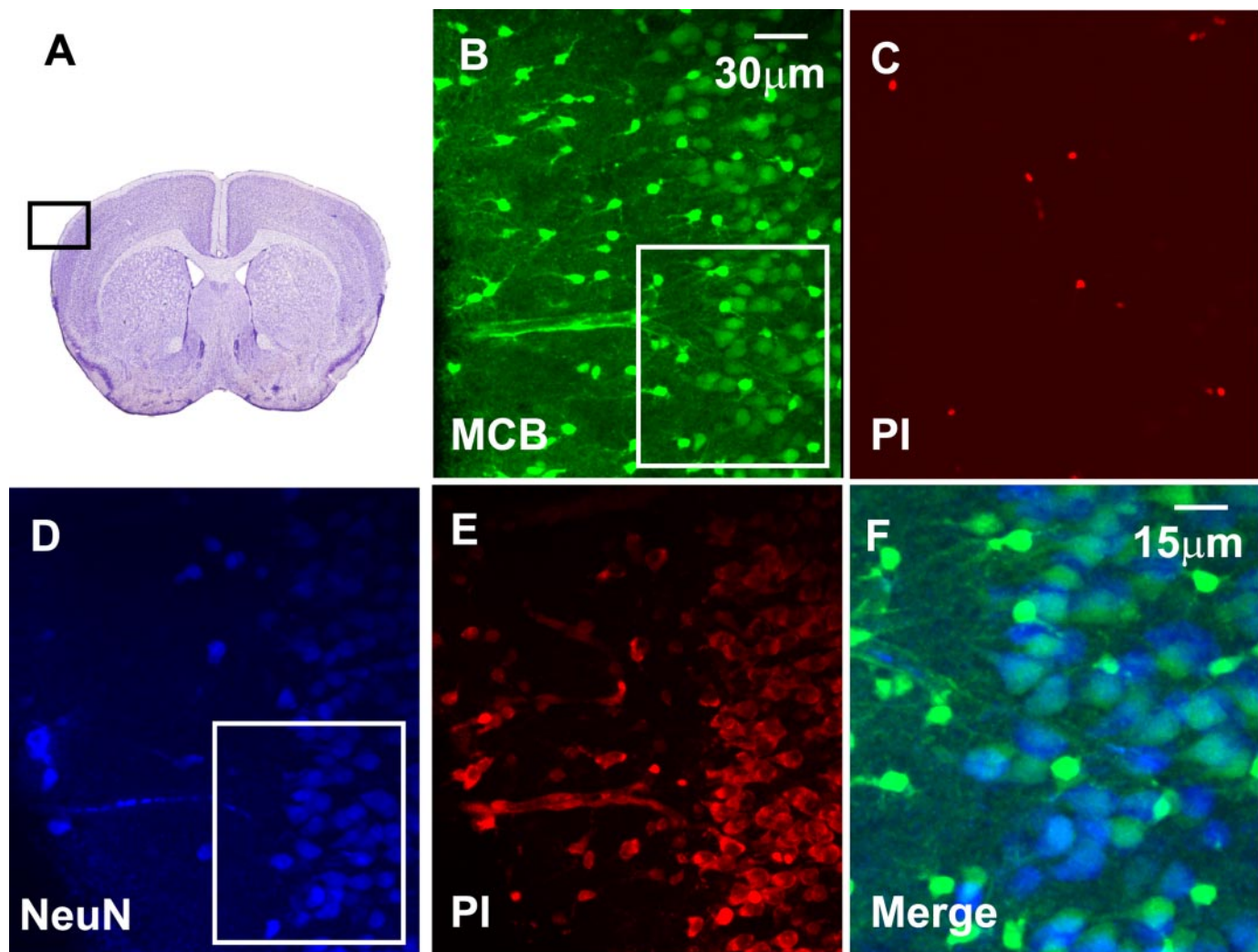


FIGURE 3. Relatively weak MCB labeling of mature cortical neurons. *A*, coronal section of the rat brain showing the location of two-photon imaging, modified from Ref. 84. *B*, MCB labeling of cortical layers I and II in a rat brain slice. In layer II, there are many cells with neuronal morphology labeled by MCB, with much lower fluorescence intensity than the MCB-labeled astrocytes in layer I. *C*, PI labeling of the same region as *B* in an acute slice, showing dead cells with ruptured membranes permeable to PI (membranes of healthy cells are normally impermeable to PI). *D*, immunostaining of the same region in *A* with NeuN, a neuron-specific nuclear protein (primary antibody) and FITC anti-mouse as the secondary antibody, showed that the cells with relatively lower fluorescence in layer II in *A* are neurons. *E*, PI labeling of the same region after fixation and PI permeation. *F*, overlay of NeuN and MCB signals (region from *inset* in *B* and *D*). Because fixation caused irregular stretching of slices and MCB staining can only be performed on live tissue, we only overlaid the inset region where cells of interest were best aligned. Images were taken using two-photon microscopy with a $\times 40$ objective.

These cells had the morphology of neurons with apical dendrites oriented toward the meninges (Fig. 3*B*). Co-labeling the acute live slices with PI showed that these cells had intact membranes, because there was no overlap between the MCB and PI signal, and were thus viable (Fig. 3*C*). After fixation with paraformaldehyde, the MCB signal was completely lost (data not shown), whereas the PI signal was preserved within cells that had died during vibratome sectioning and also spread to all fixed cells that were originally labeled by MCB, including those with neuronal morphology (Fig. 3*E*). Immunostaining with NeuN, a neuron-specific nuclear protein (37), confirmed that the cells with a lower level of fluorescence were indeed neurons (Fig. 3, *D* and *F*).

In previous studies using largely developing neurons and glia in cell culture-based assays, inferences regarding the cellular distribution of GSH in brain have been inconsistent. Some studies suggest that GSH is substantially lower in cortical neurons than in glia (38–41), although others do not (11, 42, 43). Our results provide direct evidence that in the cerebral cortex *in situ* there is heterogeneity in the distribution of GSH between neurons and glia, with neurons in general exhibiting much lower levels of GSH.

MCB Labeling of GSH Content in Mature Neurons Is Limited by GSH Precursors and Not MCB Availability—Our experiments indicate that layer II cortical neurons show a much lower level of MCB fluorescence than astrocytes. A concern is that neurons are unable to take up MCB as efficiently as astrocytes, potentially limiting neuronal GSH labeling. To address this possibility, we attempted to increase GSH synthesis by adding 30 μM NAC, a cell membrane-permeable cysteine precursor to acute slices after MCB labeling reached a plateau level (44, 45). At 50 min after NAC addition, the neuronal GSH content was elevated from 0.12 ± 0.04 to 0.42 ± 0.04 mM ($p < 0.001$; $n = 3$ separate experiments) (Fig. 4, *A–D*), whereas the astrocyte GSH content increased only marginally from 0.84 ± 0.09 to 1.19 ± 0.07 mM ($p < 0.01$; $n = 2$ separate experiments) (Fig. 4*I*). To confirm that increased MCB fluorescence increase was because of increased GSH (rather through direct conjugation with cysteine), we incubated slices in 100 μM BSO for 3 h to prevent *de novo* GSH synthesis (Fig. 4, *E–H*). BSO completely blocked the NAC-mediated increase in neuronal and astrocyte MCB labeling (Fig. 4*J*). These results suggest that neurons have apparently lower MCB-GSH fluorescence than astrocytes because of a limitation in GSH precursor (cysteine) availability, rather than MCB uptake or GST activity. There-

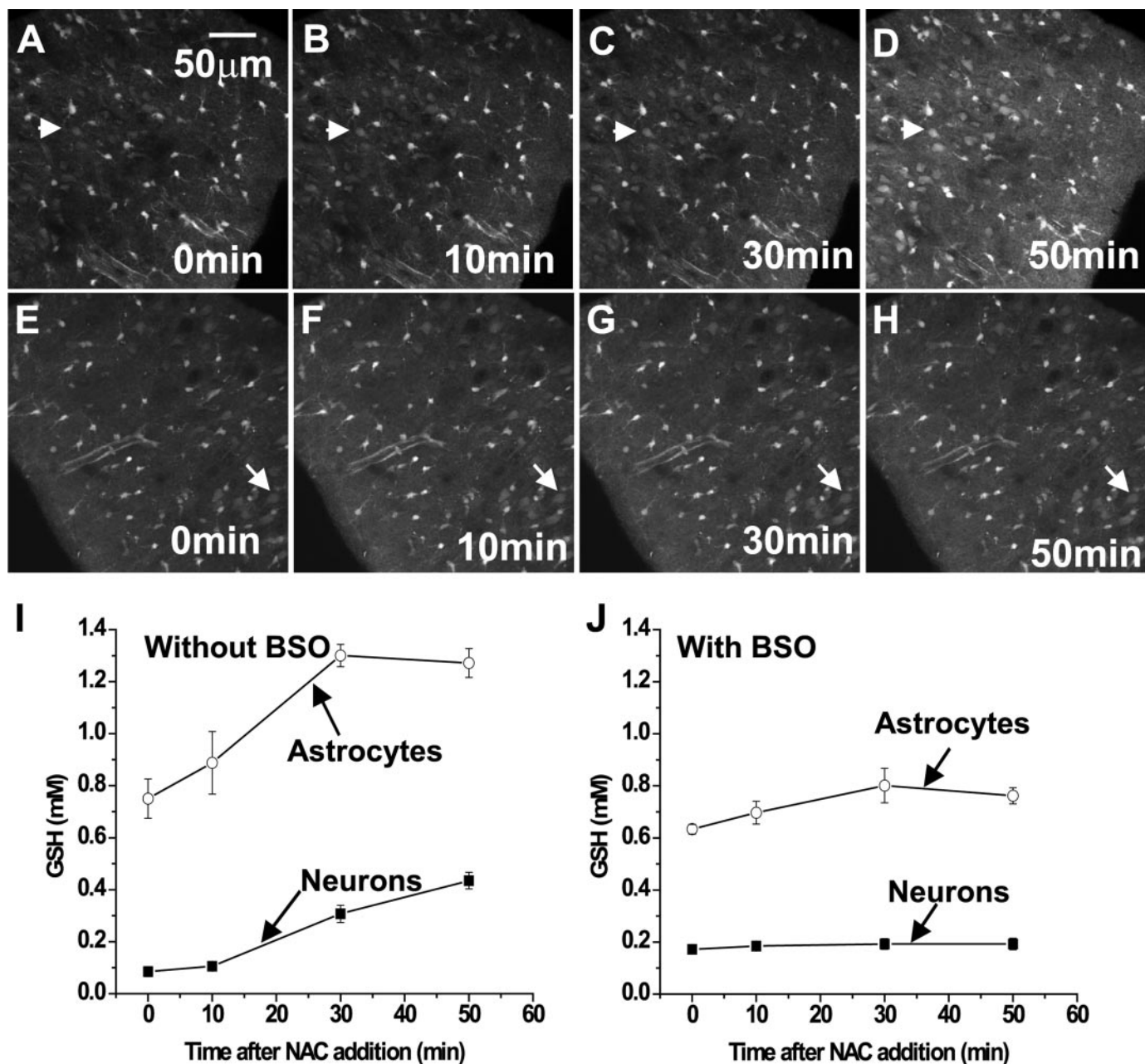


FIGURE 4. Neuronal GSH content can be increased by a cell-permeable cysteine precursor indicating that MCB levels are not limiting. *A*, MCB labeling within a cortical brain slice from a P15 rat. *B–D*, two-photon images taken 10, 30, and 50 min after $30 \mu\text{M}$ NAC were added to the slice. *E*, MCB labeling of a P15 rat slice incubated in $100 \mu\text{M}$ BSO for 3 h. *F–H*, two-photon images were taken at 10, 30, and 50 min after $30 \mu\text{M}$ NAC was added to the BSO-treated slice. Images were taken using two-photon microscopy with a $\times 40$ objective. Arrows indicate neurons at different time points. *I* and *J*, time course of MCB-GSH fluorescence in neurons and astrocytes after NAC addition with and without BSO addition as indicated (data from a single experiment is shown).

fore our data indicating that mature neurons only contain $0.1\text{--}0.2 \text{ mM}$ GSH reflects their actual GSH concentration.

Lateral Ventricle Ependymal Cells Have the Highest GSH Content in Brain Slices—In addition to meningeal cells and astrocytes, MCB also strongly labeled ependymal cells along the lateral ventricle (Fig. 5*A*). These cells were significantly brighter than any other region of brain slices examined (Fig. 7*A*). As with the meninges, ependymal cells also face CSF and are known to express a high level of cystine-glutamate transporter xCT, allowing the extraction of cystine for GSH synthesis (36). Ependymal cells may also contribute to maintenance of brain redox homeostasis by synthesizing and exporting GSH. In close proximity to ependymal cells is the subventricular zone where neurogenesis can occur (even in mature brain) (46). Cells within the subventricular

zone were also strongly labeled by MCB (Fig. 5*B*). Immunostaining with double cortin (DCX), which is expressed in migrating and differentiating immature neurons (47, 48), suggested that many of these GSH-containing subventricular zone cells are neuronal precursor cells (Fig. 5, *C* and *D*).

A Subpopulation of Developing Neurons in Dentate Gyrus Are Labeled by MCB—Previous studies using mercury orange histochemistry imply that developing neurons may exhibit and require higher levels of GSH (40). However, this reagent lacks the enzyme-based specificity of GST-mediated MCB labeling of GSH and may have been a general thiol indicator. Initially we examined brain slices from young (P1–2) rats and found cells of presumably neuronal origin to have high GSH content (data not shown). However, in these young animals it was difficult

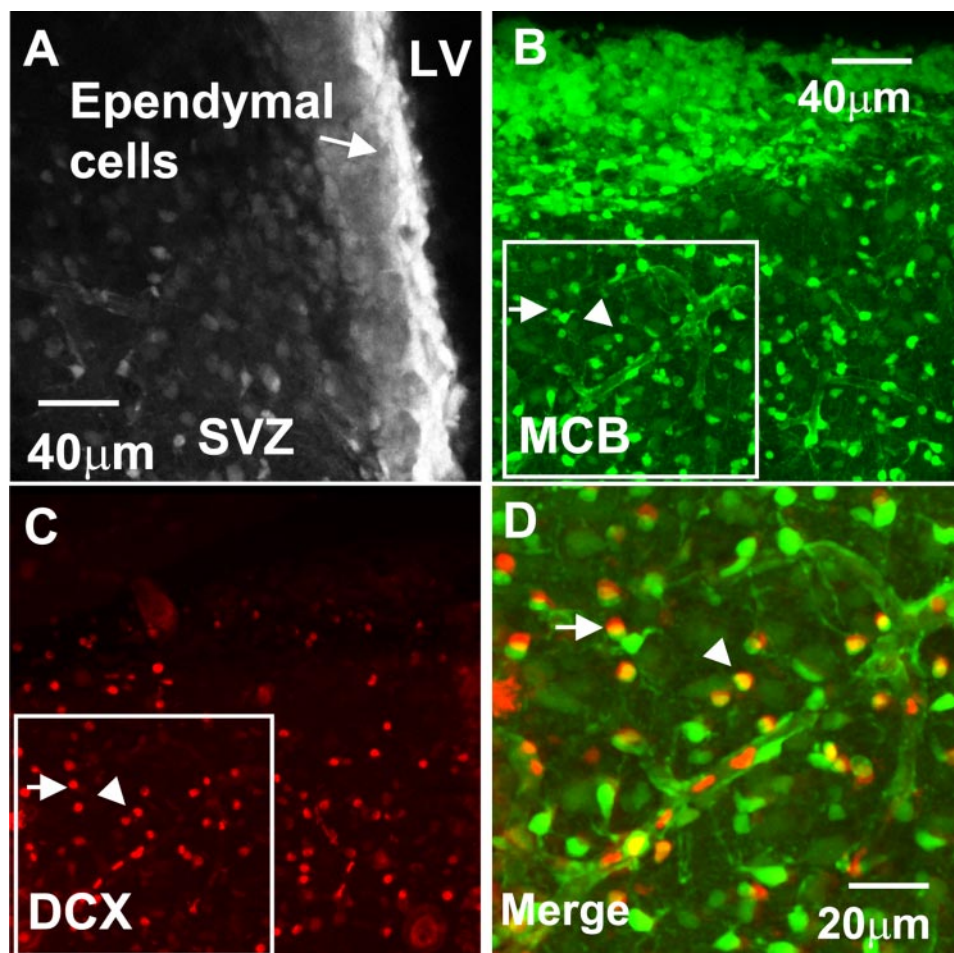


FIGURE 5. MCB labeling of GSH-containing ependymal cells lining the lateral ventricle. *A*, ependymal cells lining the lateral ventricle show very strong fluorescence after MCB labeling. Although lower in fluorescence than the ependymal layer, cells within the subventricular zone (SVZ) were clearly labeled by MCB. *B*, MCB labeling along lateral ventricle from another slice. *C*, DCX staining of the same region as in *B*. *D*, overlay of MCB and DCX signals (region from inset in *B* and *C*). The arrow and arrowhead point to two cells in subventricular zone that are labeled both by MCB and DCX. Note the distortion due to comparing live MCB labeled and fixed immunostained slices. Images were taken with $\times 40$ objective.

to co-stain MCB-labeled neurons with antibody markers because the neurons were not fully differentiated, and the morphology of the slices was greatly altered by fixation. Furthermore, it was conceivable that the properties and viability of young slices might be quite different from those of mature animals thus making direct comparisons difficult.

Given the high levels of GSH in the lateral ventricle ependymal cells and associated subventricular zone and their potential role in neurogenesis, we also examined GSH-bimane labeling in other neurogenic zones such as hippocampal dentate gyrus. Granule neurons of different developmental stages are found within medial and lateral aspects of the granule cell layers (49). The most strongly MCB-labeled cells were located at the border between the condensed granular cell layer and the hilus (also termed subgranular layer; see Fig. 6, *A–D*) and were negative for the mature neuronal marker NeuN. Cells at this subgranular location may be dividing precursor cells that have a unique immunocytochemical profile (50, 51); they are expected to be DCX-positive but NeuN and glial fibrillary acidic protein-negative. 55% of MCB-labeled cells were labeled by DCX (Fig. 6, *E–H*; $n = 225$ cells from two separate animals). This suggests that a high level of GSH may be required to support the high proliferation rate and consequent elevated metabolic activity of these precursor cells. Lateral to the highly fluorescent group of cells (within the condensed granular cell layer), we found a population of cells labeled weakly by both MCB and NeuN, a marker for mature neurons (Fig. 6, *C* and *D*). The most lateral group of cells in the granular cell layer was not labeled by MCB but strongly labeled by NeuN (Fig. 6, *C* and *D*). PI labeling of the live slices showed that the majority of these cells in the granular cell layer had intact membranes and were presumably viable because there was an absence of overlap between MCB and

PI signals (data not shown). Because newborn granular cells are first present in the inner granular cell layer and migrate to the outer portion as they develop (49), and the levels of NeuN are correlated with the extent of differentiation (37), we conclude that neurons gradually reduce their GSH content as they mature.

Measurement of GSH Concentration in Different Brain Regions in Acute Brain Slices—Our data indicate that the fluorescence intensity of GSH-MCB is directly proportional to GSH concentration (Fig. 1*B*). Therefore, when the MCB reaction reaches a plateau, we can estimate intracellular GSH concentration in brain slices. Our measurement is based on two assumptions. First, there is little efflux of GSH-MCB from brain slices at room temperature under the conditions our experiments were performed. As mentioned above, cells can export the GSH-MCB conjugates through a family of Mrps (22, 52). We have previously examined the efflux of GSH-MCB through Mrps in astrocyte cultures and found that 75% of GSH-MCB conjugate is exported at 37 °C within 10 min (13). In contrast, at room temperature efflux was reduced considerably (13). We further tested whether Mrp1-mediated efflux played a significant role in brain slices by adding 50 mM MK571 (21), and we compared the fluorescence intensity after MCB labeling with control slices. Addition of MK571 produced no significant change in labeling of neurons and glia ($p > 0.05$ from five separate slice experiments). We also washed slices with fresh ACSF after MCB labeling reached a plateau level (in the absence of MK571), and we did not find significant reduction in fluorescence intensity after washing ($p > 0.05$ from two separate slice experiments). The slice washing experiment suggested that non-MK571-sensitive efflux mechanisms for MCB conjugates were minor. All of the above indicated that in brain slices at room temperature the

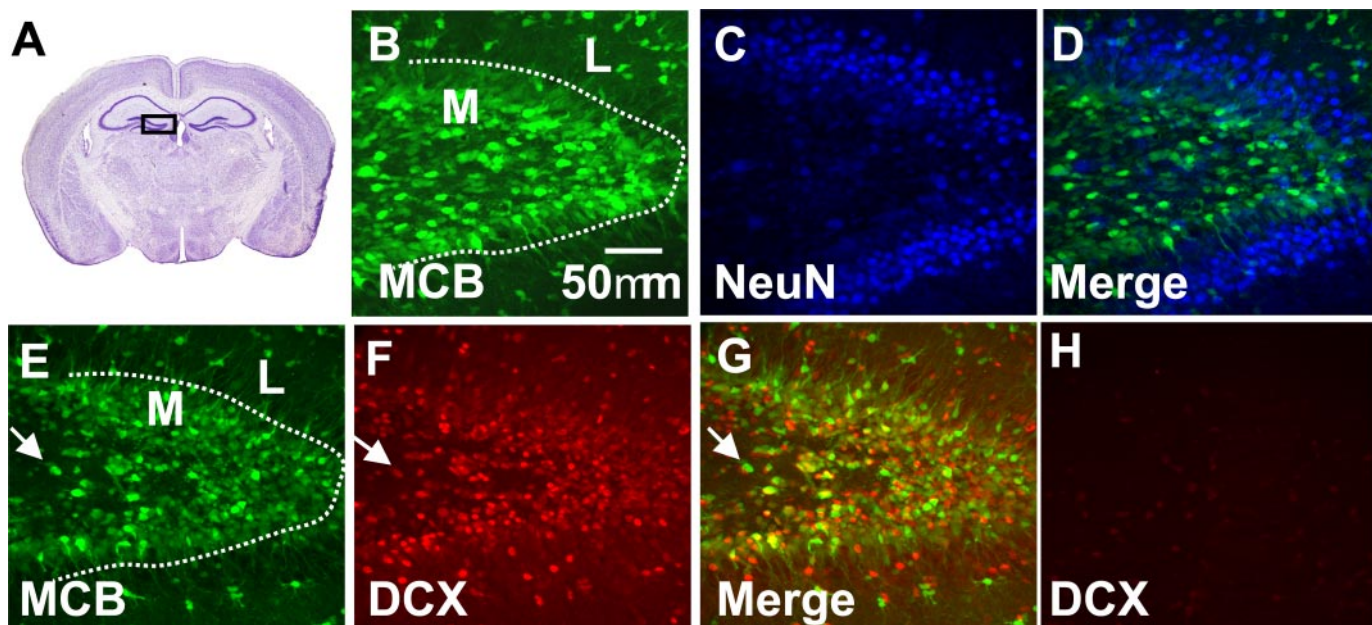
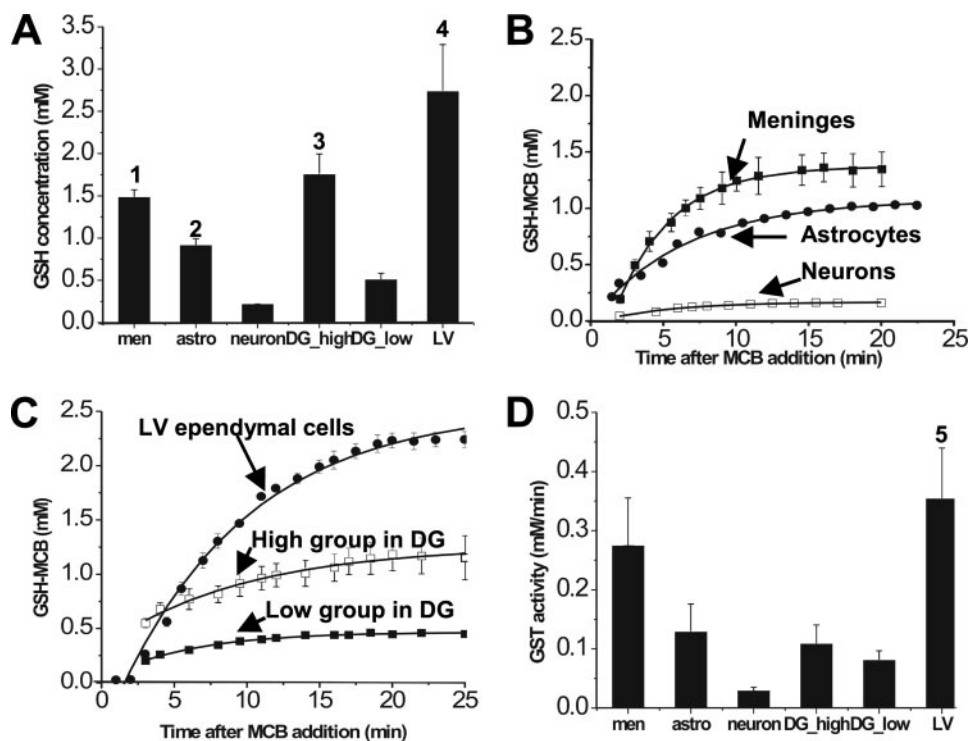


FIGURE 6. MCB labeling of GSH-containing cells in dentate gyrus. *A*, coronal section of the rat brain showing location of two-photon imaging, modified from Ref. 84. *B*, MCB labeled two groups of cells in dentate gyrus. Cells within subgranular cell layers (border between condensed granular cell layer and hilus) showed relatively higher fluorescence, whereas cells within the medial granular cell layer (*M*) showed lower fluorescence. Cells deep within the lateral portion of the granular cell layer (*L*) were unlabeled by MCB (not significantly above background neuropil) and appeared as *black holes*. *C*, NeuN staining of the same slice showing that the dark voids (no MCB label) in the outer portion of granular cell layer are viable NeuN-positive neurons, and by using PI staining on the live slice we confirmed that these unlabeled NeuN-positive neurons were not dead. *D*, overlay of MCB and NeuN signal showed that the cells in the lateral portion of granular cell layer that were not labeled by MCB could be labeled by NeuN. *E*, MCB labeling of dentate gyrus in another slice. *F*, DCX staining of the same region as in *E*. *G*, overlay of DCX and MCB signal. *H*, DCX staining within the hippocampal CA1 region where little neurogenesis occurs, showing that DCX staining in the subgranular zone is specific for progenitor cells. Images were all taken with $\times 40$ objective.

FIGURE 7. Quantification of GSH concentration in different brain regions. *A*, GSH concentrations in different regions of P15 to P21 rat brain slices. Data for different brain regions were averaged from five experiments as follows: 1, $p < 0.001$, significantly higher GSH in meninges (*men*) when compared with astrocytes (*astro*) and neurons; 2, $p < 0.001$, when astrocytes were compared with neurons; 3, $p < 0.01$, subgranular layer dentate gyrus cells (high fluorescence) contain significantly higher GSH when compared with the more lateral dentate gyrus cells found in the granule cell layer (low fluorescence); 4, $p < 0.05$, lateral ventricle (*LV*) ependymal cells contain more GSH than all other cell types examined. *B* and *C*, time course curves of MCB labeling of meninges, cortical astrocytes, cortical neurons, high fluorescence cells of dentate gyrus (subgranule layer presumed neuronal progenitors), low fluorescence cells in dentate gyrus (medial granule layer presumed neurons), and ependymal cells along the lateral ventricle. Data points were averaged from five cells within a single slice. *D*, the MCB conjugation activity (proportional to GST activity) in different brain regions estimated from the exponential fitting of the time course curves. Average values from three separate experiments are shown. There was a trend but no significant difference in conjugation activity between meninges, astrocytes, and neurons. 5, $p < 0.05$ lateral ventricle ependymal cells had significantly higher GST activity than all other cell types except meninges. Data given as mean \pm S.E. and analyzed with repeated measures one-way analysis of variance.



efflux of GSH-MCB by MK571-sensitive Mrp1 is negligible. The second assumption is that during each experiment we have allowed the reaction between MCB and GSH to proceed until completion, and thus GST activity is not limiting (even in experiments with neurons). In plots of MCB fluorescence intensity *versus* time peak MCB labeling occurs within 20 min in all cell types examined, including differentiated cortical layer II neurons (Fig. 7, *B* and *C*). We further tested this by adding

more MCB to slices after the fluorescence had reached the plateau level, and we found no further increase in fluorescence intensity, indicating that MCB is in excess and presumably labels all intracellular GSH (data not shown).

We next measured the GSH concentration in different brain regions by converting the plateau level of fluorescence to a GSH concentration with the standard curve (Fig. 7*A*). In order to standardize for effects of

Imaging Glutathione in Intact Brain Indicates Redox Buffers

imaging depth on fluorescence intensity (excitation and emission efficiency are reduced at greater depths) (53), we made all of the measurements from the cells at about 20–30 μm below the surface of the slice. By surveying various brain regions, we found that lateral ventricle ependymal cells show the highest level of GSH ($2.73 \pm 0.56 \text{ mM}$, $p < 0.05$ when compared with all other brain regions measured), which is consistent with their potential role in regulating the redox state of the CSF system. The GSH level in meningeal cells was significantly higher than in cortical astrocytes (meninges, $1.45 \pm 0.09 \text{ mM}$; astrocytes, $0.91 \pm 0.08 \text{ mM}$, $p < 0.001$). Because astrocytes have been described as a crucial part of antioxidant defense in brain cells (28, 31), our finding suggests that meninges that have received little attention in this context so far may also be an important component of the brain antioxidant system. The GSH level in astrocytes is about five times greater than that of cortical layer II neurons (astrocytes, $0.91 \pm 0.08 \text{ mM}$; neurons, $0.21 \pm 0.02 \text{ mM}$, $p < 0.001$), suggesting that neighboring astrocytes support neuronal viability by releasing GSH during oxidative stress. When multiple cell types were compared in tissues, we always made paired measurements for the various cell types examined at each respective depth to prevent errors in assessment of fluorescence associated with variation in imaging depth (see “Discussion” for assessment of error). In dentate gyrus, the presumed neuronal progenitors (based on cell position and staining with markers) express a relatively high level of GSH ($1.75 \pm 0.24 \text{ mM}$), and differentiated dentate gyrus neurons contained significantly lower concentrations ($0.50 \pm 0.08 \text{ mM}$, $p < 0.01$).

As mentioned in Fig. 1, because MCB is in excess and the conjugation between GSH and MCB can be regarded as a first-order reaction, the time course curve should fit a single exponential. Fig. 7, B and C, shows the time courses of MCB labeling in meninges, cortical astrocytes, cortical neurons, progenitor cells in dentate gyrus, young neurons in dentate gyrus, and lateral ventricle ependymal cells, respectively. All of these curves were described by a single exponential function and reached a plateau level after labeling for 20 min, again indicating that GST activity was not limiting and that MCB staining reflects GSH content. These curves can be fitted well with Equation 1 above. We assume that the initial slope of the curve reflects GST activity in these cells (Fig. 7D) and indicates that it was not limiting in any of the cell types examined. In addition, experiments showing that the cysteine precursor NAC can increase MCB labeling of neurons also supports the proposal that GSH synthesis and not GST activity determines apparent differences in GSH levels between the cell types examined (Fig. 4). Within the dentate gyrus, the putative progenitor cells based on their subgranular position were termed high fluorescence group, whereas the medial young neurons of the granule cell layer (weakly NeuN-positive) were termed low fluorescence group; the lateral granule layer neurons (outer region of layer) were only weakly labeled by MCB and were not plotted. Within the dentate gyrus two major groups (low and high fluorescence) were apparent based on NeuN expression; the group with a lower NeuN level corresponded to higher a GSH-MCB. In assessing the mean GSH level within these populations, we observed no overlap in GSH concentrations and little variability (Fig. 7A). To determine whether these cells represent two distinct populations, we examined the GSH-MCB levels from 66 cells within an experiment and put them into 17 different intensity bins. We then fit the resulting histogram, which had two distinct peaks, to one or two Gaussian distributions and found a significantly better fit for 2 Gaussians ($R^2 = 0.82$) versus a single Gaussian distribution ($R^2 = 0.08$), suggesting that there were two distinct populations of cells differentially labeled by NeuN and MCB.

MCB Labels a Subpopulation of Meningeal and Neocortical Cells in Vivo—It is conceivable that GSH metabolism in slices may be different from that *in vivo* for a variety of reasons, including the lack of slice blood supply and exposure to blood-derived GSH precursors as well as the possibility of trauma in making brain slices. With two-photon *in vivo* microscopy, we were able to image GSH distribution in the intact brain directly (Fig. 8, A–F). Exposure of the cortical surface of anesthetized mice to MCB resulted in staining of a subpopulation of neocortical cells with a plateau level of fluorescence reached in 30 min (Fig. 8G). In these experiments, small cranial windows ($2 \times 2 \text{ mm}$) were made on C57Bl/6 mice, and 100 μM MCB was applied directly to the somatosensory cortex surface, and MCB-containing agarose was then layered over the brain surface to mechanically stabilize it and to continuously supply MCB for on-going labeling. MCB-labeled cells were imaged up to 250 μm below the brain surface. At the surface, MCB labeled many apparently meningeal cells (Fig. 8A). Side view projections (to examine tissue below the surface meninges) demonstrated that in the neocortex all the MCB-labeled cells were of astroglial morphology (Fig. 8E). These cells have multiple processes originating from the cell body, often forming end feet attached to unstained blood vessels (Fig. 8C, arrow). In *in vivo* experiments we did not include MK571, and the preparation was at 37 $^{\circ}\text{C}$, so we expect the plateau level of fluorescence reached to reflect the steady state balance between GSH synthesis and efflux (Fig. 8G). Recently, Nimmerjahn *et al.* (54) have demonstrated that SR 101 can be a relatively specific marker of astroglia in the neocortex *in vivo*. In these experiments SR 101 co-localized with astrocyte markers in neocortex but failed to stain neurons, microglia, or oligodendrocytes. By co-labeling with MCB and SR 101 *in vivo* and collecting the signal from the green and red channels, respectively, we found that these two probes labeled the same population of astrocyte-like cells in the cortical parenchyma (Fig. 8D). The meningeal cells labeled by MCB can also be labeled by SR 101 (Fig. 8B). These results are consistent with our data from cortical slices where MCB robustly labels both the meninges and astrocytes. A three-dimensional projection from the side view of the *in vivo* data stack showed that both in layer I (~ 0 to approximately $-130 \mu\text{m}$) and layer II (begins at approximately $-130 \mu\text{m}$), MCB-labeled cells are astrocytes as they are co-labeled by SR 101 (Fig. 8F). No neurons in layer II (SR 101-negative cells) were detected by this approach using the mature mice that we studied (>2 months of age). However, we have found that neurons in brain slices from young rats (less than 3 weeks) can be labeled by MCB, although with a very low fluorescence level ($\sim 20\%$ of astrocyte levels). The reason why neurons are not labeled *in vivo* cannot be due to a lack of MCB tissue penetration, because astrocytes at the same depth level as neurons can be labeled. Perhaps in brain slices less attenuation of fluorescence signals takes place allowing the observation of layer II neurons. It is also possible that the slices from young rats (P15 to P21) contain more immature neurons that have relatively higher GSH. Consistent with this, using the Tietze assay (23) we have seen higher GSH levels in tissue homogenates from young and embryonic rats than compared with adults.⁵ Although SR 101 labeled the same population of cells as MCB *in vivo*, not all fluorescent indicators label only this population. In our hands and in previous work (54) calcium green 1-AM robustly labels layer II neurons (as well as glia) and thus has a different pattern of labeling than MCB (data not shown), indicating specificity of MCB and SR 101 labeling. We also considered whether SR 101 might be trapped within cells by the same mechanism as MCB (GST catalyzed GSH-conjugate), but we failed to find that SR 101 was a GST substrate suggesting that SR 101 and MCB both label astrocytes, albeit by different mechanisms. These controls add support to the

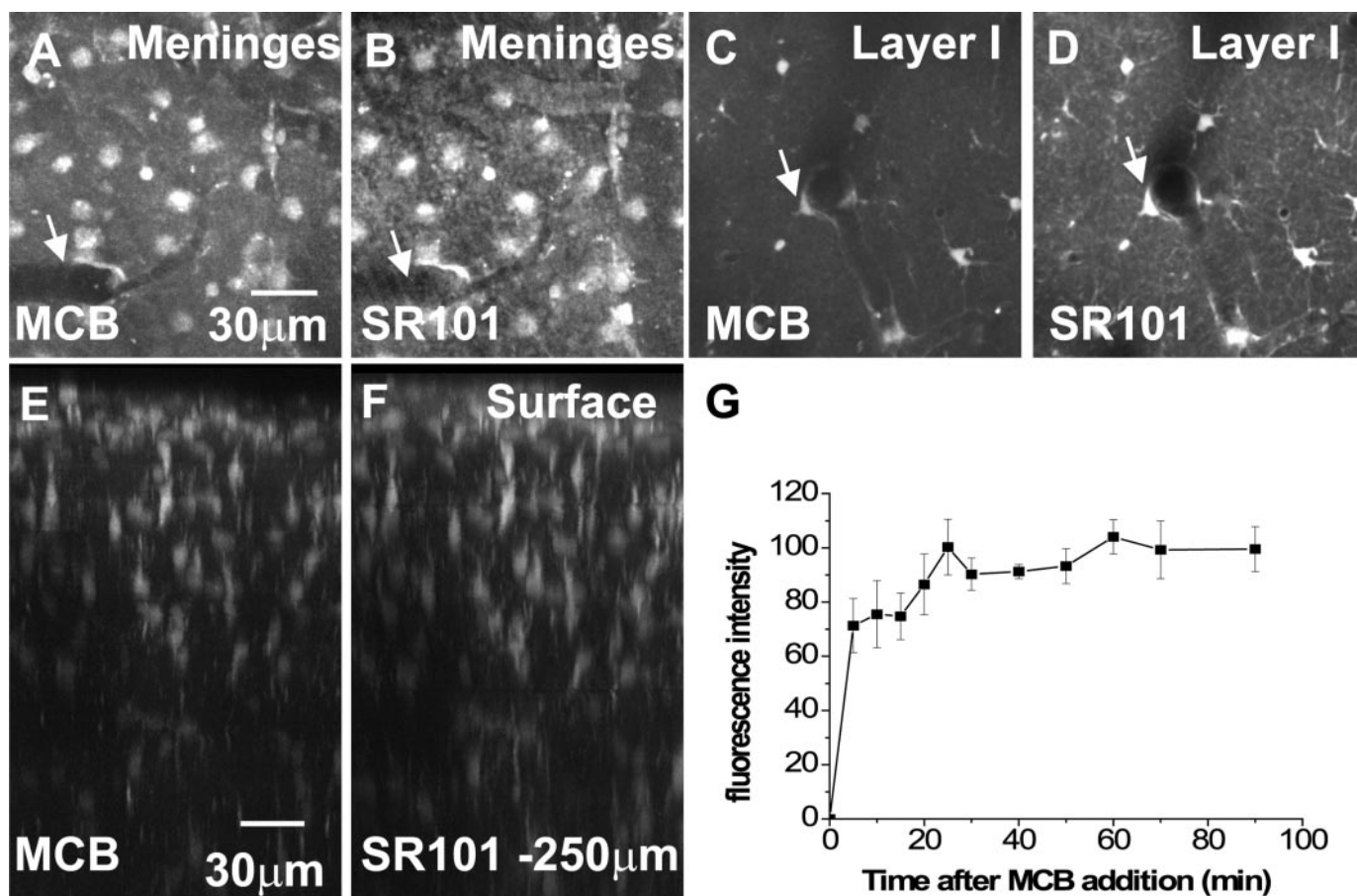


FIGURE 8. *In vivo* two-photon fluorescence image of the somatosensory cortex of a live anesthetized mouse after application of MCB and SR 101. *A*, image recorded at the brain surface after MCB labeling. A population of meningeal cells are labeled by MCB. Blood vessels appear as dark gaps (arrow). *B*, SR 101 labeling of the same region as in *A*. MCB and SR 101 labeled the same group of cells. *C*, optical section of MCB fluorescence recorded about 50 μm below the pial surface showing that a subpopulation of cells had taken up the dye deeper within the parenchyma. These cells had astroglial morphological features and some formed end feet surrounding unstained blood vessels (arrow). *D*, optical section of fluorescence for the astrocyte marker SR 101 (applied to the brain surface simultaneously with MCB) in the same region as *C*. *E*, side view (*X-Z* image) of the MCB-labeled meninges and astrocytes in neocortex (maximal intensity projections) from the surface of the brain to a depth of approximately $-250 \mu\text{m}$, reconstructed from planar scans acquired every 1 μm after MCB addition. *F*, side view of SR 101-labeled cells in meninges and neocortex. All images were taken with $\times 40$ objective. *G*, time course curve of MCB *in vivo* labeling showing that the fluorescence intensity reaches a plateau level within 30 min. Average values from three different experiments are shown.

argument that addition of MCB to the cortex *in vivo* largely labels astrocytes because they contain high levels of GSH.

DISCUSSION

MCB Labeling with Two-photon Microscopy Resolves Cellular GSH in Situ—Accumulating evidence indicates that alteration of GSH content and oxidative stress play substantial roles in neurological disorders such as stroke, Parkinson, Alzheimer, and Huntington disease (1–3, 55–57). In view of the pivotal role of GSH in protecting cells (10, 31, 58), there has been interest in methods to quantify GSH content by using biochemical assays (23, 59, 60). However, biochemical assays using cell lysates or tissue homogenates are unsuitable for examining GSH levels in intact cells. Immunostaining with antibodies against GSH suffers from potential alterations in GSH disposition in response to fixation (11). The ability to measure GSH at the cellular level using two-photon imaging overcomes limitations inherent with conventional biochemical and histochemical techniques and reveals a marked cellular heterogeneity in labeling patterns lost in a biochemical assay for GSH. However, it is important to note that light scattering by tissues limits the depth of two-photon microscopy to $\sim 500 \mu\text{m}$ (53, 61). When measuring GSH concentration in slices, we standardized for the effect of depth by measuring the fluorescence intensity of all regions at similar depths approximately -20 – $30 \mu\text{m}$. At this level, damage caused by tissue sectioning is

negligible, and this image depth would be expected to have similar (attenuating) effects on MCB fluorescence in different brain regions. Brain slice experiments by Oheim *et al.* (53) and Helmchen and Denk (61) found that fluorescence emission produced by 800 nm two-photon excitation would be reduced by 20–30% for tissue depths ranging from 20 to 30 μm below the surface (based on a length constant of 87 μm for brain slices of similar age to what we used). According to Kleinfeld and Denk (16), two-photon fluorescence intensity decreased by $\sim 50\%$ at 100 μm in rats *in vivo*; therefore, at the depths where we made our measurements light attenuation will have minimal effects and cannot account for the large differences in GSH levels between cell types. It is conceivable that not all cellular organelles handle GSH-MCB equally and that there could be some sequestration or exclusion of label. This does not seem to be a serious problem because optical sectioning failed to reveal heterogeneity in labeling subcellularly. Importantly, we have shown that comparison of the MCB-GSH two-photon imaging method to the biochemical assay of GSH gives proportional results (Fig. 1C). These findings suggest that probe saturation, binding, and detector saturation are not serious limitations using the cells and conditions we employ. Another potential caveat is that the MCB-GSH labeling technique is a means of measuring the total GSH content of a cell of interest (by converting all GSH to a fluorescent MCB conjugate) and will not necessarily provide a real time sensor of GSH levels. To measure GSH

Imaging Glutathione in Intact Brain Indicates Redox Buffers

content at different time points within the same preparation one would need to 1) load and measure GSH-MCB content, 2) allow for efflux of GSH-MCB, and 3) reload with MCB. If reloading is done in the presence of GSH precursors, the rate of GSH synthesis/precursor uptake can also be measured as we have done with astrocyte cultures (13). It is conceivable that a reloading procedure could be used on brain slices or *in vivo* preparations at physiological temperature where MCB-GSH efflux would be accelerated. Although these limitations exist and are acknowledged to aid future researchers, we feel that two-photon imaging of MCB labeling in brain slices is an improvement over previously employed biochemical or imaging assays for GSH.

Cellular GSH Distribution in Brain Slices—It has been well established that heterogeneity in GSH levels exists between neurons and astrocytes in brain parenchyma (28). However, the relationship between GSH concentration in neurons *versus* astrocytes has not been consistent between all studies (40, 41, 43). These differences may in part be related to the developmental state or culture conditions of the preparations used. Interestingly, of all regions studied, lateral ventricle ependymal cells contain the highest level of GSH. Also of note, the meninges contain considerably higher GSH than neocortical astrocytes. Sato *et al.* (36) have reported that xCT (a high affinity cystine uptake system) is highly expressed both in meninges and in ependymal cells. Both of these regions are in direct contact with CSF making them ideally positioned to take up cystine for GSH synthesis and release it to protect the brain against oxidative stress. The meninges have received little attention in antioxidant defense and have mainly been highlighted for their physical role at the CSF-blood barrier (34, 62, 63). Our findings provide a new insight into the possible role of the meninges in protecting the brain against oxidative stress.

We have also used relatively pure *in vitro* cultures of astrocytes and meningeal cells to more clearly evaluate the antioxidant functions of MCB-labeled cells. In additional studies (83),⁵ we found that cultured meningeal cells possess higher levels of xCT-mediated cystine uptake and exhibit increased GSH synthesis after exposure to Nrf2-inducing electrophilic agents, when compared with astrocytes. This finding is consistent with the high level of meningeal MCB labeling observed in our imaging experiments here (Fig. 7, A and B). Strikingly, when co-cultured with neurons, meningeal cells are even more efficient in conferring neuroprotection against oxidative stress-dependent glutamate toxicity than astrocytes (13). These results suggest that *in vivo*, all of the highly MCB-labeled cells we have identified (meninges, ependyma, and astrocytes) could contribute to redox buffering and positively influence neuronal survival.

In addition to the non-neuronal cell types mentioned above, developing neurons in mature brain contained high GSH-MCB levels consistent with *in vitro* work showing a requirement for high levels of thiol precursors in young neurons for survival (64). In the mature brain there are two major regions where neurogenesis is known to occur postnatally, the subventricular zone and the subgranular zone of the dentate gyrus (50). Our results indicate that both neurogenic regions contain relatively high levels of GSH. In dentate gyrus, young neurons in the medial (inner) portion of granular cell layer contain GSH at a level much lower than the dividing precursor cells (subgranular zone), whereas the mature neurons in the lateral (outer) portion of the granular cell layer contain only background levels of GSH. This suggests that when neurons are proliferating they are in great need of an antioxidant buffer and thus contain high GSH. We propose that during the process of maturation, neurons lose most of their GSH content and henceforth seem to depend on astrocytes to provide them with this antioxidant buffer. This is consistent with the findings of Beiswanger *et al.* (40) who visualized

GSH distribution in the mouse nervous system by mercury orange histochemistry, which detects cellular thiols (largely GSH), and suggested that all neuronal and glial progenitor cells contain GSH, whereas most neurons lose the bulk of their GSH content by P5. Other groups also reported that neurons lose their GSH content as they grow in co-culture with astrocytes (55, 65). This low level of GSH content in mature neurons may explain their unique vulnerability to oxidative stress (64, 66–69). Given the high metabolic rate of mature neurons, it is surprising that they have little GSH and would apparently rely on astrocyte GSH to derive precursors such as reduced cysteine to synthesize their own moderate levels of GSH. Astrocyte are thought to release GSH which is broken down extracellularly into cysteine and taken up by neurons for thiol synthesis and utilization (54). Perhaps mature neurons operate with a small GSH buffer because they are under continuous metabolic pressure or alternatively they function at a more oxidized reducing potential because it is optimal for a signaling or metabolic process.

Measurement of GSH within the Cortex of Live Animals—Brief exposure of the intact brain to MCB followed by two-photon imaging proved to be a robust method for labeling GSH-containing cells in the somatosensory cortex *in vivo*. The specificity of MCB labeling for astrocytes in neocortex was verified by co-labeling with an astrocyte marker (54). This approach offers the opportunity to measure GSH content in live animals. The GSH antioxidant system can be activated when the brain is under oxidative stress, such as during the reperfusion period after an ischemic insult when GSH demand may be relatively higher (70, 71). It will also be affected by many neurological disorders, such as Parkinson disease (72) and Alzheimer disease (73). Recent data also indicate a role for GSH and its precursors in maintaining the viability of brain tumors (74). However, in most cases data linking the GSH system to these disorders were derived from tissue homogenates, which cannot detect cellular heterogeneity. It is possible that these limitations may have contributed to contrary reports on how the GSH levels change during some neurological diseases (75–78). Our approach can be applied to animal models of disease and mouse mutants with abnormal handling of oxidative stress (79, 80) to measure GSH levels in different brain regions directly. Recent studies from our laboratory have used electrophilic inducers of the redox-sensitive transcription factor Nrf2 to induce multiple antioxidant systems as a therapeutic strategy for stroke (56, 57). In future studies, MCB-GSH could be used to image and quantify the cellular sites of GSH induction by Nrf2 inducers, as well as other manipulations that influence the GSH system (81, 82). Recently, we (14) and others (81, 82) have used two-photon microscopy to investigate the effect of both local and widespread blockade of cortical vessels on brain structure after stroke. Our approach to measure GSH levels *in vivo* combined with two-photon microscopy of blood flow and structure may provide unique insight into how the brain deals with the oxidative stress after stroke.

In conclusion, we have developed an approach to image GSH content in intact brain tissue. Based on inferences made from these imaging experiments, we report the unexpected finding that meningeal and lateral ventricle ependymal cells may play a large role in brain redox homeostasis.

REFERENCES

- Schulz, J. B., Lindenau, J., Seyfried, J., and Dichgans, J. (2000) *Eur. J. Biochem.* **267**, 4904–4911
- Bains, J. S., and Shaw, C. A. (1997) *Brain Res. Brain Res. Rev.* **25**, 335–358
- Perry, G., Avila, J., Espy, M. G., Wink, D. A., Atwood, C. S., and Smith, M. A. (2001) *Science* **291**, 595–597
- Kamencic, H., Griebel, R. W., Lyon, A. W., Paterson, P. G., and Juurlink, B. H. (2001) *FASEB J.* **15**, 243–250

5. Liu, T. H., Beckman, J. S., Freeman, B. A., Hogan, E. L., and Hsu, C. Y. (1989) *Am. J. Physiol.* **256**, H589–H593
6. Kinouchi, H., Epstein, C. J., Mizui, T., Carlson, E., Chen, S. F., and Chan, P. H. (1991) *Proc. Natl. Acad. Sci. U. S. A.* **88**, 11158–11162
7. Yu, Z. F., Bruce-Keller, A. J., Goodman, Y., and Mattson, M. P. (1998) *J. Neurosci. Res.* **53**, 613–625
8. Chatterjee, S., Noack, H., Possel, H., Keilhoff, G., and Wolf, G. (1999) *Glia* **27**, 152–161
9. Meyer, A. J., and Fricker, M. D. (2000) *J. Microsc. (Oxf)* **198**, 174–181
10. Cooper, A. J., and Kristal, B. S. (1997) *Biol. Chem.* **378**, 793–802
11. Hjelle, O. P., Chaudhry, F. A., and Ottersen, O. P. (1994) *Eur. J. Neurosci.* **6**, 793–804
12. Wang, X. F., and Cynader, M. S. (2000) *J. Neurochem.* **74**, 1434–1442
13. Sun, X., Erb, H., and Murphy, T. H. (2005) *Biochem. Biophys. Res. Commun.* **326**, 371–377
14. Zhang, S., Boyd, J., Delaney, K., and Murphy, T. H. (2005) *J. Neurosci.* **25**, 5333–5338
15. Kleinfeld, D., Mitra, P. P., Helmchen, F., and Denk, W. (1998) *Proc. Natl. Acad. Sci. U. S. A.* **95**, 15741–15746
16. Kleinfeld, D., and Denk, W. (2000) in *Imaging Neurons: A Laboratory Manual* (Yuste, R., Lanni, F., and Konnerth, A., eds) pp. 23.1–23.15, Cold Spring Harbor Laboratory Press, Cold Spring Harbor, NY
17. Cook, J. A., Iype, S. N., and Mitchell, J. B. (1991) *Cancer Res.* **51**, 1606–1612
18. Ublacker, G. A., Johnson, J. A., Siegel, F. L., and Mulcahy, R. T. (1991) *Cancer Res.* **51**, 1783–1788
19. Meyer, A. J., May, M. J., and Fricker, M. (2001) *Plant J.* **27**, 67–78
20. Hayes, J. D., Flanagan, J. U., and Jowsey, I. R. (2005) *Annu. Rev. Pharmacol. Toxicol.* **45**, 51–88
21. Hirrlinger, J., Schulz, J. B., and Dringen, R. (2002) *J. Neurosci. Res.* **69**, 318–326
22. Borst, P., Evers, R., Kool, M., and Wijnholds, J. (1999) *Biochim. Biophys. Acta* **1461**, 347–357
23. Tietze, F. (1969) *Anal. Biochem.* **27**, 502–522
24. St John, P. A., Kell, W. M., Mazzetta, J. S., Lange, G. D., and Barker, J. L. (1986) *J. Neurosci.* **6**, 1492–1512
25. Matthias, K., Kirchoff, F., Seifert, G., Huttmann, K., Matyash, M., Kettenmann, H., and Steinhauser, C. (2003) *J. Neurosci.* **23**, 1750–1758
26. Walz, W., and Lang, M. K. (1998) *Neurosci. Lett.* **257**, 127–130
27. Anderson, M. F., Blomstrand, F., Blomstrand, C., Eriksson, P. S., and Nilsson, M. (2003) *Neurochem. Res.* **28**, 293–305
28. Dringen, R. (2000) *Prog. Neurobiol.* **62**, 649–671
29. Iwata-Ichikawa, E., Kondo, Y., Miyazaki, I., Asanuma, M., and Ogawa, N. (1999) *J. Neurochem.* **72**, 2334–2344
30. Chen, Y., Vartiainen, N. E., Ying, W., Chan, P. H., Koistinaho, J., and Swanson, R. A. (2001) *J. Neurochem.* **77**, 1601–1610
31. Shih, A. Y., Johnson, D. A., Wong, G., Kraft, A. D., Jiang, L., Erb, H., Johnson, J. A., and Murphy, T. H. (2003) *J. Neurosci.* **23**, 3394–3406
32. Kraft, A. D., Johnson, D. A., and Johnson, J. A. (2004) *J. Neurosci.* **24**, 1101–1112
33. Ghersi-Egea, J. F., Leninger-Muller, B., Suleman, G., Siest, G., and Minn, A. (1994) *J. Neurochem.* **62**, 1089–1096
34. Tanno, H., Nockels, R. P., Pitts, L. H., and Noble, L. J. (1993) *J. Cereb. Blood Flow Metab.* **13**, 116–124
35. McKinnon, S. G. (1998) *Neuroimaging Clin. N. Am.* **8**, 101–117
36. Sato, H., Tamba, M., Okuno, S., Sato, K., Keino-Masu, K., Masu, M., and Bannai, S. (2002) *J. Neurosci.* **22**, 8028–8033
37. Mullen, R. J., Buck, C. R., and Smith, A. M. (1992) *Development (Camb)* **116**, 201–211
38. Slivka, A., Mytilineou, C., and Cohen, G. (1987) *Brain. Res.* **409**, 275–284
39. Lowndes, H. E., Beiswanger, C. M., Philbert, M. A., and Reuhl, K. R. (1994) *Neurotoxicology* **15**, 61–73
40. Beiswanger, C. M., Diegmann, M. H., Novak, R. F., Philbert, M. A., Graessle, T. L., Reuhl, K. R., and Lowndes, H. E. (1995) *Neurotoxicology* **16**, 425–440
41. Tauskela, J. S., Hewitt, K., Kang, L. P., Comas, T., Gendron, T., Hakim, A., Hogan, M., Durkin, J., and Morley, P. (2000) *Glia* **30**, 329–341
42. Amara, A., Coussemacq, M., and Geffard, M. (1994) *Brain Res.* **659**, 237–242
43. Rice, M. E., and Russo-Menna, I. (1998) *Neuroscience* **82**, 1213–1223
44. Aruoma, O. I., Halliwell, B., Hoey, B. M., and Butler, J. (1989) *Free Radic. Biol. Med.* **6**, 593–597
45. Aoyama, K., Suh, S. W., Hamby, A. M., Liu, J., Chan, W. Y., Chen, Y., and Swanson, R. A. (2006) *Nat. Neurosci.* **9**, 119–126
46. Doetsch, F., and Alvarez-Buylla, A. (1996) *Proc. Natl. Acad. Sci. U. S. A.* **93**, 14895–14900
47. Brown, J. P., Couillard-Despres, S., Cooper-Kuhn, C. M., Winkler, J., Aigner, L., and Kuhn, H. G. (2003) *J. Comp. Neurol.* **467**, 1–10
48. Francis, F., Koulakoff, A., Boucher, D., Chafey, P., Schaar, B., Vinet, M. C., Friocourt, G., McDonnell, N., Reiner, O., Kahn, A., McConnell, S. K., Berwald-Netter, Y., Denoulet, P., and Chelly, J. (1999) *Neuron* **23**, 247–256
49. Kempermann, G., Gast, D., Kronenberg, G., Yamaguchi, M., and Gage, F. H. (2003) *Development (Camb.)* **130**, 391–399
50. Li, G., and Pleasure, S. J. (2005) *Dev. Neurosci.* **27**, 93–99
51. Kempermann, G., Jessberger, S., Steiner, B., and Kronenberg, G. (2004) *Trends Neurosci.* **27**, 447–452
52. Leslie, E. M., Deeley, R. G., and Cole, S. P. (2001) *Toxicology* **167**, 3–23
53. Oheim, M., Beaurepaire, E., Chaigneau, E., Mertz, J., and Charpak, S. (2001) *J. Neurosci. Methods* **111**, 29–37
54. Nimmerjahn, A., Kirchhoff, F., Kerr, J. N., and Helmchen, F. (2004) *Nat. Methods* **1**, 31–37
55. Keelan, J., Allen, N. J., Antcliffe, D., Pal, S., and Duchon, M. R. (2001) *J. Neurosci. Res.* **66**, 873–884
56. Shih, A. Y., Imbeault, S., Barakauskas, V., Erb, H., Jiang, L., Li, P., and Murphy, T. H. (2005) *J. Biol. Chem.* **280**, 22925–22936
57. Shih, A. Y., Li, P., and Murphy, T. H. (2005) *J. Neurosci.* **25**, 10321–10335
58. Herzenberg, L. A., De Rosa, S. C., Dubs, J. G., Roederer, M., Anderson, M. T., Ela, S. W., and Deresinski, S. C. (1997) *Proc. Natl. Acad. Sci. U. S. A.* **94**, 1967–1972
59. Anderson, M. E. (1985) *Methods Enzymol.* **113**, 548–555
60. Newton, G. L., Dorian, R., and Fahey, R. C. (1981) *Anal. Biochem.* **114**, 383–387
61. Helmchen, F., and Denk, W. (2005) *Nat. Methods* **2**, 932–940
62. Nilsson, C., Lindvall-Axelsson, M., and Owman, C. (1992) *Brain Res. Brain Res. Rev.* **17**, 109–138
63. Smith, G. M., and Shine, H. D. (1992) *Int. J. Dev. Neurosci.* **10**, 387–392
64. Murphy, T. H., Schnaar, R. L., and Coyle, J. T. (1990) *FASEB J.* **4**, 1624–1633
65. Sagara, J. I., Miura, K., and Bannai, S. (1993) *J. Neurochem.* **61**, 1672–1676
66. Bolanos, J. P., Heales, S. J., Land, J. M., and Clark, J. B. (1995) *J. Neurochem.* **64**, 1965–1972
67. Dringen, R., Kussmaul, L., Gutterer, J. M., Hirrlinger, J., and Hamprecht, B. (1999) *J. Neurochem.* **72**, 2523–2530
68. Schubert, D., and Piasecki, D. (2001) *J. Neurosci.* **21**, 7455–7462
69. Ratan, R. R., Murphy, T. H., and Baraban, J. M. (1994) *J. Neurochem.* **62**, 376–379
70. Lyrer, P., Landolt, H., Kabiersch, A., Langemann, H., and Kaeser, H. (1991) *Brain Res.* **567**, 317–320
71. Rehncrona, S., Folbergrova, J., Smith, D. S., and Siesjo, B. K. (1980) *J. Neurochem.* **34**, 477–486
72. Schapira, A. H., Cooper, J. M., Dexter, D., Clark, J. B., Jenner, P., and Marsden, C. D. (1990) *J. Neurochem.* **54**, 823–827
73. Abramov, A. Y., Canevari, L., and Duchon, M. R. (2003) *J. Neurosci.* **23**, 5088–5095
74. Chung, W. J., Lyons, S. A., Nelson, G. M., Hamza, H., Gladson, C. L., Gillespie, G. Y., and Sontheimer, H. (2005) *J. Neurosci.* **25**, 7101–7110
75. Mizui, T., Kinouchi, H., and Chan, P. H. (1992) *Am. J. Physiol.* **262**, H313–H317
76. Guegan, C., Ceballos-Picot, I., Nicole, A., Kato, H., Onteniente, B., and Sola, B. (1998) *Exp. Neurol.* **154**, 371–380
77. Uemura, Y., Miller, J. M., Matson, W. R., and Beal, M. F. (1991) *Stroke* **22**, 1548–1553
78. Gotoh, O., Yamamoto, M., Tamura, A., and Sano, K. (1994) *Acta Neurochir.* **60**, (suppl.) 318–320
79. Aoyama, K., Suh, S. W., Hamby, A. M., Liu, J., Chan, W. Y., Chen, Y., and Swanson, R. A. (2006) *Nat. Neurosci.* **9**, 119–126
80. Siddiq, A., Ayoub, I. A., Chavez, J. C., Aminova, L., Shah, S., Lamanna, J. C., Patton, S. M., Connor, J. R., Cherny, R. A., Volitakis, I., Bush, A., Langsetmo, I., Seeley, T., Gunzler, V., and Ratan, R. R. (2005) *J. Biol. Chem.* **280**, 41732–41743
81. Nishimura, N., Schaffer, C. B., Friedman, B., Tsai, P. S., Lyden, P. D., and Kleinfeld, D. (2006) *Nat. Methods* **3**, 99–108
82. Schaffer, C. B., Friedman, B., Nishimura, N., Schroeder, L. F., Tsai, P. S., Ebner, F. F., Lyden, P. D., and Kleinfeld, D. (2006) *PLoS Biol.* **4**, 258–270
83. Sun, X., et al. (2005) *Soc. Neurosci. Abstr.* 221.14
84. Paxinos, G., and Watson, C. (1986) *The Rat Brain in Stereotaxic Coordinates*, Academic Press, San Diego